An Experimental Investigation of Crack-path Directional Stability

A photoelastic and experimental study on the effect of crack-tip stress biaxiality with respect to directional stability and fracture toughness of Mode I crack extension

by R. Streit and I. Finnie

ABSTRACT—Using the criterion that a crack will extend perpendicular to the maximum circumferential stress, σ_θ, we show that the directional stability of crack growth is governed by the location of microcrack initiation ahead of the crack tip. At distances greater than a geometrical radius r_0, the maximum value of σ_θ deviates from the position of symmetry. Thus, if we assume that the physical processes involved in fracture lead to crack initiation at a distance r_c ahead of the crack tip, the criterion for directional stability is $r_0 > r_c$. Experimental and theoretical values of r_0 verify that, as r_0 becomes small, the crack's directional stability deteriorates.

Observing that a lengthwise compressive stress increases r_0, a center-cracked specimen was developed which allows the application of controlled lengthwise compression independently of the opening-mode load. A detailed photoelastic analysis of the specimen has provided the value of r_0 as a function of the crack length. The value of r_0 is then compared with the expected microcrack initiation distances in ductile fracture.

By applying sufficient lengthwise compression, we are able to make the crack grow straight and obtain numerous data points from this specimen which would otherwise be directionally unstable. The results indicate that, as the total lengthwise tensile stress at the crack tip increases, the fracture toughness also increases. Using this information we can then adjust K_{Ic} for zero lengthwise loading and obtain a geometry independent fracture toughness.

Nomenclature

A_2 = constant second term of crack-tip stress series (Pa)
CCS = center-crack specimen
CT = compact tension
DCB = double-cantilever beam
K_I = stress-intensity factors for Mode I loading. Singularity term of crack-tip stress-series solution (MPa-m$^{1/2}$)
$Q(\theta_f)$ = function of θ_f for photoelastic use
r, θ = polar-coordinate system centered at crack tip. Direction of crack propagation along $\theta = 0$ deg
r_c = critical distance in front of the crack tip where crack initiation occurs (m)
r_f = photoelastic-fringe radius (m)
r_0 = maximum radius for which the maximum σ_θ lies on $\theta = 0$ deg (m)
θ_f = photoelastic-fringe angle for $(\partial\tau_m)/(\partial\theta) = 0$
$\sigma_r, \sigma_\theta, \tau_\theta$ = crack-tip stresses referred to polar-coordinate system (Pa)
τ_m = maximum shear stress for a given point (Pa)

Introduction

In order to obtain Mode I fracture-toughness data, the crack must propagate along the plane of symmetry of the test specimen. Two methods have been employed to control the crack direction when loaded in Mode I. The commonly used scheme to ensure directional stability is to side groove the test piece.[1] However, this creates a complex state of stress on the specimen surface[2] and may force the crack to grow in an unnatural, but straight, direction.

The second method involves the application of a compressive stress parallel to the plane of the crack.[3] It has been demonstrated that sufficient lengthwise compression ensures directional stability.[4,5] Our current work investigates two aspects of this stabilizing effect.

Using the theory that the direction of crack growth is governed by the orientation of the maximum circumferential stress, we first develop a stability requirement using photoelasticity. By analyzing the isochromatic-fringe geometry in the vicinity of the crack tip we can determine if the specimen will be directionally stable. Further, we then use the photoelastic results to investigate how a lengthwise load influences the crack-tip stress field.

It is difficult to apply a pure lengthwise compression (and thus ensure directional stability) on most common fracture specimens. In double-cantilever beam-type specimens, for example, the lengthwise loading generally influences the opening load and may also introduce

R. Streit (SESA Member) is Engineer, Lawrence Livermore Lab., Livermore, CA 94550. I. Finnie (SESA Member) is Professor, University of California, Berkeley, CA 94720.

Paper was presented at 1979 SESA Spring Meeting held in San Francisco, CA on May 20-25.

Original manuscript submitted: May 18, 1979. Final version received: August 16, 1979.

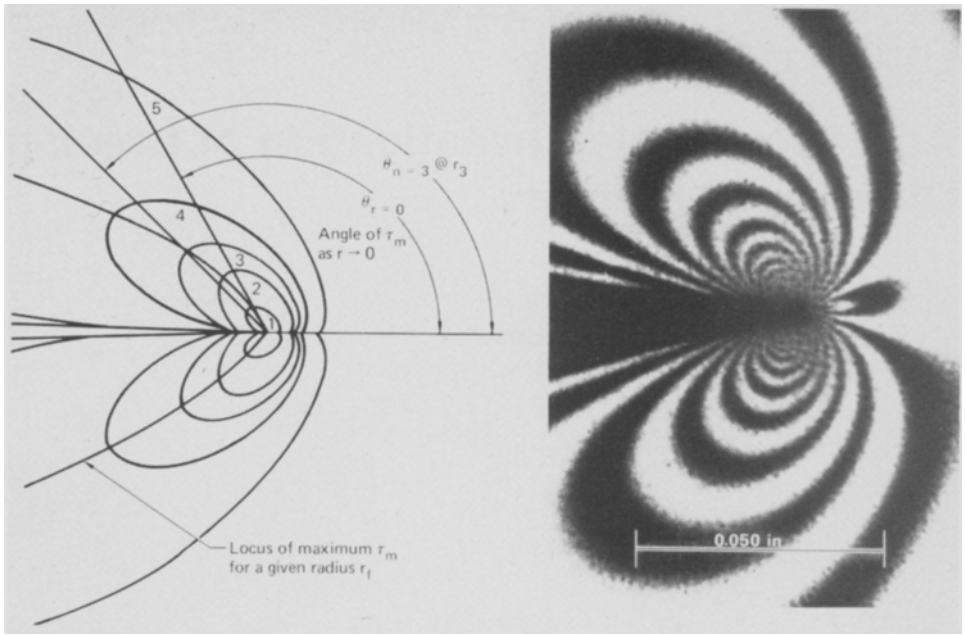

Fig. 1—Photoelastic stress field at the tip of sharp crack

unwanted moments. Therefore, a new specimen was developed which allows application of a controlled lengthwise stress independently of the opening-mode load. Using this specimen, we investigate the influence of lengthwise loading on directional stability.

In effect, the externally applied lengthwise stress changes the constant second term in the series expansion of the elastic-stress field around a crack. The influence of this term on measured fracture-toughness values is seldom considered. With the present apparatus, we are able to study this factor and present results for 7075-T651 aluminum.

Theoretical-stability Model

Many theories have been proposed to predict the direction of crack extension for an arbitrarily oriented crack. Predictions have been made using energy-release criteria, stress models, and strain-energy-density concepts for both kinked and unkinked crack-tip configurations. For our present discussion, it is sufficient to note that all these methods lead to very similar predictions—particularly in the case of predominantly Mode I loading. As scatter is inherent to the theories on crack-growth direction due to low stress and energy gradients in the critical direction, the conceptual simplicity and applicability of the maximum σ_θ theory makes its use totally acceptable. Thus, using the original Erdogan and Sih[6] proposal—that crack growth will occur normal to the maximum σ_θ—with subsequent improvements to examine the stress field a short distance ahead of the crack,[7,8] we now turn our attention to predicting the directional stability of crack growth. Since the vast majority of fracture tests involve Mode I loading, our focus will be restricted to this case, i.e., $K_{II} = 0$.

Considering only the singularity and second-order terms in the series expansion for the stresses near a Mode I crack, the angle for which σ_θ is a maximum is defined by

$$\left[\frac{3\cos(\theta/2)\sin\theta}{8(2\pi r)^{1/2}}\right] K_I - (\sin\theta\cos\theta)\,A_2 = 0. \quad (1)$$

In this equation, K_I is the familiar singularity coefficient, A_2 is the coefficient of the second-order term and r and θ are polar coordinates centered on the crack tip. The A_2 term represents a stress applied parallel to the crack plane, i.e., a lengthwise stress. To incorporate the A_2 term, we assume that fracture initiates at a given distance ahead of the crack tip. Such a critical distance model has been shown to be physically reasonable by many authors.[9,10] Thus, although the distance at which we evaluate σ_θ may be small, r is not equal to zero.

The solution to eq (1) indicates that the maximum σ_θ need not coincide with $\theta = 0$. For $r > r_0$, where $r_0 = [9/(128\pi)](K_I/A_2)^2$, the maximum circumferential stress will deviate from the position of symmetry. Assuming that fracture initiates at a distance r_c, then the stability requirement for straight-crack growth is

$$r_0 \geq r_c.$$

Photoelastic-stability Determination

The 'stability distance' r_0 can be determined if the coefficients K_I and A_2, or their ratio is known. However, very few values of A_2 have been reported for the specimens used in fracture testing. Therefore, the value of A_2 must be evaluated by numerical or experimental methods. It will be shown that the 'stability ratio' K_I/A_2 can be determined using photoelasticity.

Using the singularity and second-order stress terms, the maximum shear stress, τ_m, in the vicinity of the crack tip is given by,

$$(2\tau_m)^2 = \frac{K_I^2\sin^2\theta}{2\pi r} - \frac{2K_IA_2\sin\theta\sin(3\theta/2)}{(2\pi r)^{1/2}} + A_2^2. \quad (2)$$

Constant values of this maximum shear stress will describe the isochromatic fringes near the tip of a sharp crack. Figure 1 shows a typical fringe pattern observed and defines the associated terms.

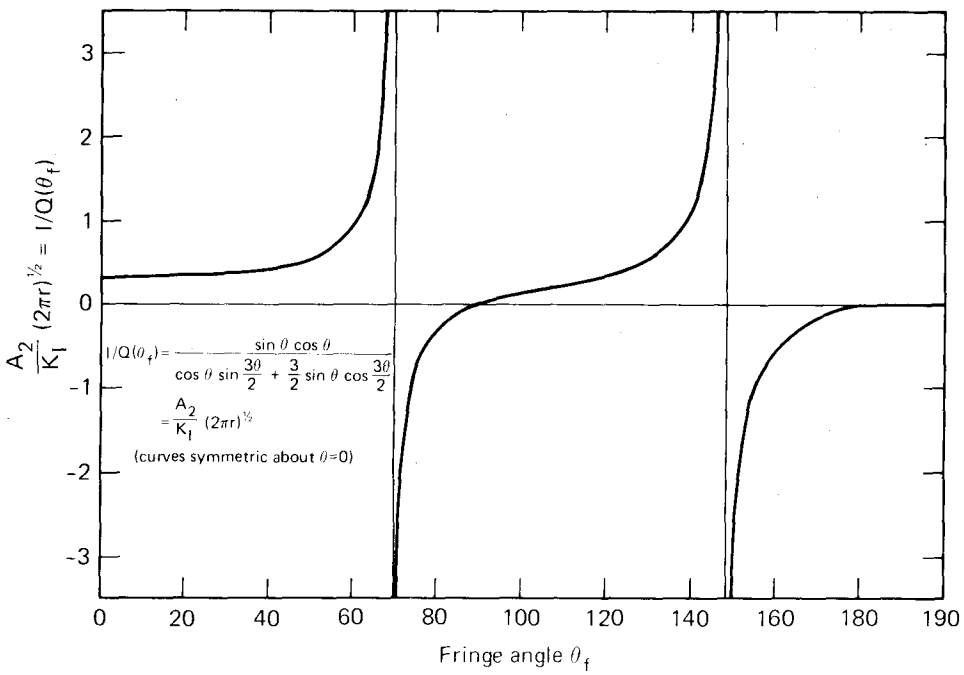

Fig. 2—Fringe angle vs. geometrical fringe constant $1/Q(\theta_f)$. Curve indicates limits on θ_f

For a given fringe loop, Irwin[11] observed that the maximum radius, r_f, can be determined by solving for the location of the maximum shear stress with respect to θ, i.e., $\partial\tau_m/\partial\theta = 0$.

In a similar manner, we can evalute the ratio K_I/A_2 if r_f and θ_f are known. Thus, differentiating eq (2) and equating to zero, we find,

$$\frac{K_I}{A_2} = \left[\frac{\sin(3\theta_f)\cos\theta_f + 3/2\sin\theta_f\cos(3\theta_f/2)}{\sin\theta_f\cos\theta_f}\right](2\pi r_f)^{1/2}. \quad (3)$$

It is interesting to note that the determination of the stability ratio requires information on the fringe geometry but is independent of the photoelastic-materials fringe-optic coefficient or fringe number. The ratio K_I/A_2 is calculated for a given specimen geometry and crack length using the coordinates of the location of maximum shear stress.

Having obtained K_I/A_2, we now address the problem of determining if a specimen will be directionally stable; and if not, where the instability will occur.

For simplicity, the function of θ_f in the square brackets on the right side of eq (3) is denoted by $Q(\theta_f)$. Recalling the stability requirement, we substitute in K_I/A_2 as determined from eq (3) to develop a photoelastic-stability criterion

$$r_c \leq r_0 = \frac{9}{128\pi}[(2\pi r_f)^{1/2} Q(\theta_f)]^2$$

or

$$r_c \leq r_0 = \frac{9r_f}{64}[Q(\theta_f)]^2 . \quad (4)$$

For a given radius, r_f = 2.5 mm (0.1 in.), Saith[4] measured the angle θ_f as a function of crack length for both the compact tension and double-cantilever-beam specimens. Using these data, we can show how the radius r_0 varies as the crack grows, (Tables 1 and 2). It should be pointed out that we do not know the critical radius r_c beyond which fracture should become unstable. However, looking at the DCB results we observe that r_0 becomes very small for crack lengths of about one-half the DCB width. We expect, and indeed we find in practice, that the crack growth should become unstable in this range. The radius r_0 of the compact tension specimen, however, never became small compared to expected values of r_c. We would predict stability regardless of crack length in this specimen.

At this point, a few notes on the limitations of photoelastic methods in studying stability should be cited. In Fig. 2, we have plotted $1/Q(\theta_f)$ vs. θ_f. For values of θ_f between 69.39 deg and 148.44 deg $1/Q(\theta_f)$ is well behaved. However, at these extreme values, $1/Q(\theta_f)$ approaches $\pm\infty$. Such values are not permissible since it requires that A_2 abruptly change sign. Values of θ_f which lie outside this range necessarily reflect boundary effects or errors in measurement.

Effect of Crack-tip Radius on Fringe Pattern

In developing the equations for the photoelastic-fringe pattern in the crack-tip vicinity, we have been making the inherent assumption that the crack is ideally sharp. When working with photoelastic materials, however, we are often required to use saw-cut cracks to investigate the stress intensity and stress patterns of a given geometry. Unless great pains are taken to produce the desired crack, we often develop a small, but important, crack-tip radius.

Creager and Paris[12] have shown how the stresses near the crack tip should be modified to include the tip-radius effect.* The modified stresses are,

*In this case, the coordinate system is located a distance $\varrho/2$ behind the crack front.

TABLE 1—VARIATION OF CRITICAL RADIUS WITH CRACK LENGTH FOR AN ASTM COMPACT TENSION SPECIMEN USING PHOTOELASTICITY [r_f = 2.5 mm (0.1 in.)]

W = 3.81 cm (1.5 in.)

a, cm	a, (in.)	a/W	θ, deg*	$Q=\frac{K_I}{A_2(2\pi r_f)^{1/2}}$	r_0, cm	r_0, (in.)	r_0/W
0.95	(0.375)	0.250	99	8.705	2.71	(1.065)	0.710
1.27	(0.500)	0.333	107	5.185	0.96	(0.378)	0.252
1.59	(0.625)	0.420	110	4.512	0.73	(0.286)	0.191
1.91	(0.750)	0.500	108	4.941	0.87	(0.343)	0.229
2.22	(0.875)	0.583	103	6.460	1.49	(0.587)	0.391
2.54	(1.00)	0.667	93	22.444	18.00	(7.084)	4.723

*Reference 4

$$\sigma_{\theta\varrho} = \sigma_{\theta sharp} + \frac{K_I}{(2\pi r)^{1/2}} \frac{\varrho}{2r} \cos\theta$$

$$\sigma_{r\varrho} = \sigma_{r sharp} + \frac{K_I}{(2\pi r)^{1/2}} \frac{\varrho}{2r} \cos\frac{\theta}{2}$$

$$\tau_{r\theta\varrho} = \tau_{r\theta sharp} - \frac{K_I}{(2\pi r)^{1/2}} \frac{\varrho}{2r} \sin\frac{7\theta}{2}$$

Now, developing these equations into the isochromatic-fringe loops as we did for the sharp-crack-tip stress equations, we find

$$\frac{K_I}{(2\pi r_f)^{1/2} A_2} = \frac{\sin\frac{3\theta_f}{2}\cos\theta_f + \frac{3}{2}\sin\theta_f\cos\frac{3\theta_f}{2} - \frac{3\varrho}{2r}\sin\frac{3\theta_f}{2}}{\sin\theta_f\cos\theta_f} \tag{5}$$

This equation reduces to eq (3) by setting $\varrho = 0$.

For comparison to the sharp-crack model, we look at the fringe angle θ_f in the limit as r_f goes to ϱ, i.e., on the crack surface along the tip radius. Modifying eq (5) and applying the stability criterion, we find that straight-crack growth is ensured for

$$r_c \le \frac{9}{128\pi}(2\pi\varrho) \left[\frac{\sin\left(\frac{3\theta_f}{2}\right)\left(\cos\theta_f - \frac{3}{4}\right) + \frac{3}{2}\sin\theta_f\cos\left(\frac{3\theta_f}{2}\right)}{\sin\theta_f\cos\theta_f}\right]^2$$

or

$$r_c \le \frac{9\varrho}{64}[Q'(\theta_f)]^2. \tag{6}$$

The right side of eq (6) is simply an alternative way of determining the stability distance r_0. In Fig. 3 we have plotted eq (6) for a family of blunt-crack-tip radii.

The Center-cracked Specimen

To investigate path stability experimentally, a specimen was developed which exhibits both stable and unstable crack growth. As discussed earlier, the A_2 term represents a stress parallel to the crack plane. Thus, by modifying this lengthwise stress term with the application of an

TABLE 2—VARIATION OF CRITICAL RADIUS WITH CRACK LENGTH FOR A 12.7-cm (5.0-in.) DCB SPECIMEN. FRINGE ANGLES MEASURED FOR r_f = 2.5 mm (0.1 in.)

a, cm	a, (in.)	θ, deg†	$Q=\frac{K_I}{A_2(2\pi r_f)^{1/2}}$	r_0, cm	r_0, (in.)
1.27	(0.50)	103	4.940	8.700	(0.34300)
1.91	(0.75)	122	2.765	2.740	(0.10850)
2.54	(1.00)	132	1.716	1.050	(0.04140)
3.18	(1.25)	137	1.220	0.530	(0.02090)
3.81	(1.50)	142	0.712	0.180	(0.00713)
5.08	(2.00)	147	0.167	0.010	(0.00039)
6.35	(2.50)	149*	−0.067*	0.002	(6.3×10^{-5})
7.62	(3.00)	150*	−0.189*	0.013	(0.00050)
8.89	(3.50)	150*	−0.189*	0.013	(0.00050)
10.16	(4.00)	146	0.281	0.025	(0.00100)

*Values of θ are outside theoretical range.
†Reference 4

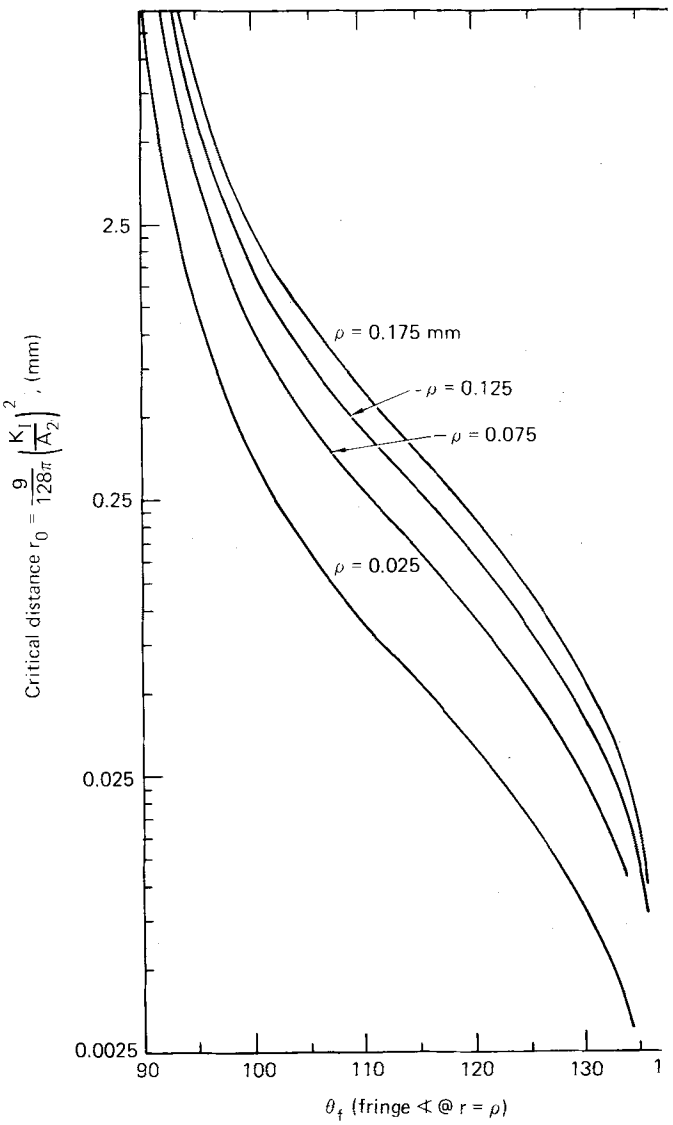

Fig. 3—Critical distance r_0 as a function of fringe angle at the surface of a rounded notch with notch radius ϱ

external lengthwise stress, we can produce a directionally stable crack. Since stability is dependent on the ratio K_I/A_2, it is desirable that the external lengthwise stress be independent of the opening-mode load. For this reason, the center-cracked specimen (CCS) was developed. The specimen used for this study was 12.7 cm (5.0 in.) long, with a height of 2.86 cm (1.125 in.). It is designed to sustain a constant lengthwise compression while being pulled by an opening load P. The specimen and test setup are shown in Fig. 4. The lengthwise compression is applied by individually adjusting four parallel tensile rods. The maximum compressive-load capability is 35.6 kN (8000 lb).

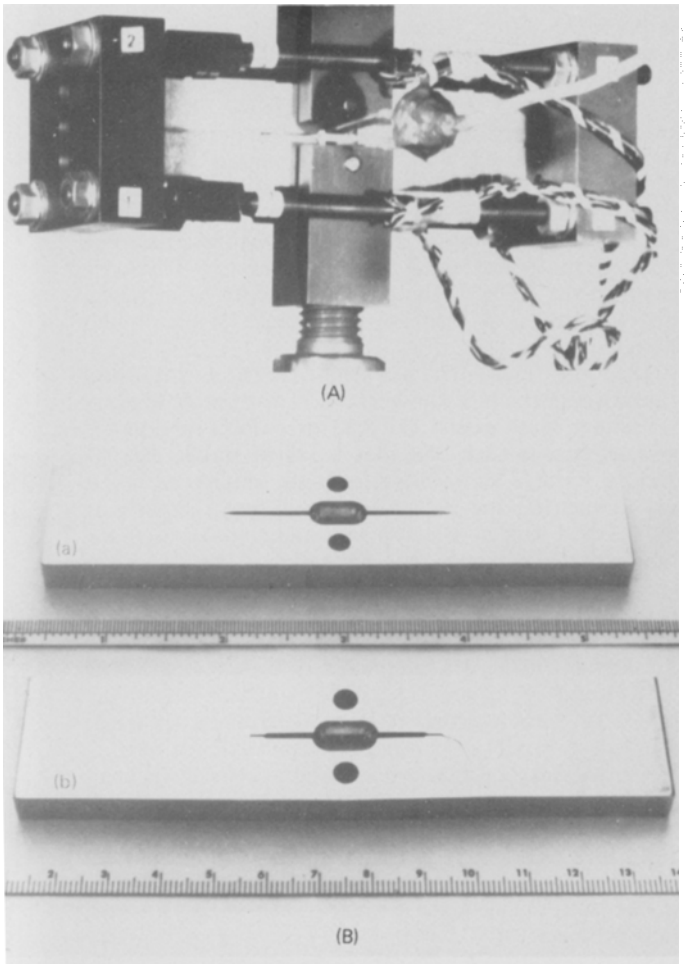

Fig. 4—Center-cracked-specimen test assembly

It was shown earlier that the isochromatic-fringe geometry can be used to determine the ratio K_I/A_2 and, therefore, r_0. Theoretically, this radius should be a constant regardless of the fringe order used to make the evaluation. However, special care must be exercised when taking measurements from the photoelastic specimens to avoid influence due to the edge effects of the crack surfaces and specimen boundary. Secondly, we must develop a sharp-crack front in the photoelastic material. This procedure involved cracking photoelastic epoxy specimens to a prescribed crack length in the CCS test apparatus. Employing the stress-freezing properties of the epoxy, the specimens were then heated to their stress-annealing temperature, deadweight loaded, and slowly cooled. The specimens were then thinned and analyzed in a modified optical comparator (set up as a magnifying polariscope). The results, showing r_0 as a function of crack length, are given in Fig. 5.

Recalling the stability criterion, the crack will grow straight if $r_0 \geq r_c$ and will become directionally unstable when $r_0 < r_c$. For example, if the crack begins to turn when $2a = 8.0$ cm (3.1 in.), Fig. 5 indicates that the critical radius $r_c = 0.14$ mm (0.0055 in.). In this manner, we can determine the crack-initiation distance, r_c, by simply observing the location of initial instability. Since r_0 is dependent on A_2, the location of instability and, thus, r_0 can be modified by the application of a lengthwise stress. By judiciously applying a lengthwise compression we can shift r_0 so as to establish path stability.

Test Results Using 7075-T651 Aluminum

Test specimens were machined from cross-rolled 7075-T651 aluminum plate. The specimen surface was lightly polished so that the crack tip could be more easily observed. Fine scribe lines were made at 3-mm (0.118-in.) intervals perpendicular to the plane of the crack to monitor crack growth.

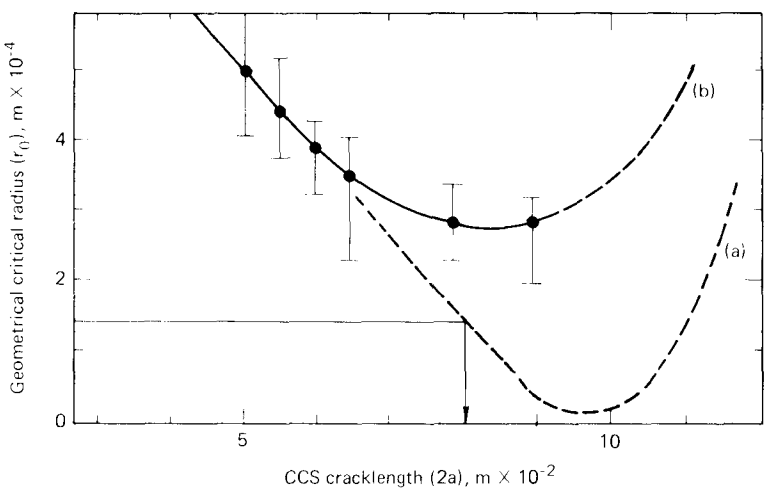

Fig. 5—Photoelastic determination of the geometrical radius r_0 for a 12.7-cm-width center-cracked specimen. The solid line shows the results of the photoelastic epoxy tests. The lower line (a) shows the expected curve for stiffer specimens. The difference occurs due to 'end effects' observed when the photoelastic specimen's elastic modulus is lowered during the stress-freezing process

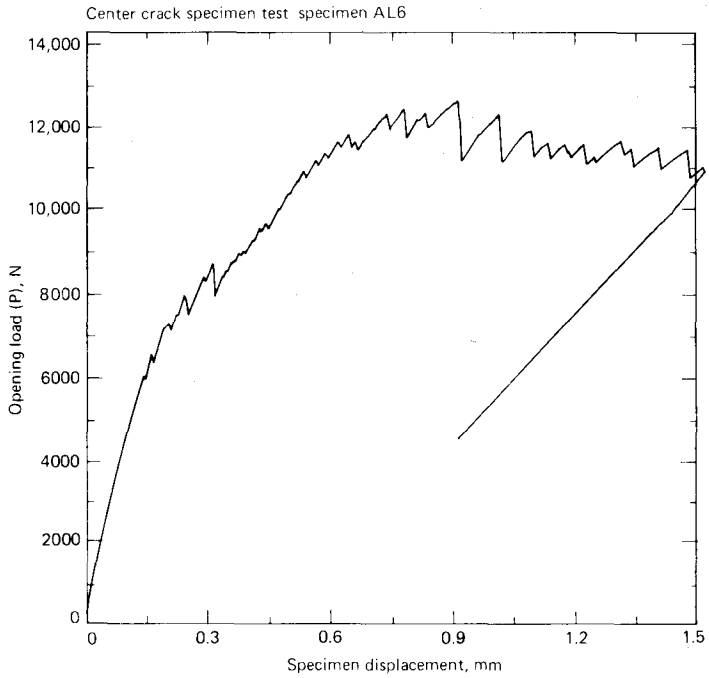

Fig. 6—Typical 7075-T6 load-displacement record

A typical load-displacement record for an aluminum specimen is shown in Fig. 6. The crack length is evaluated directly from the scribed specimen so that measurements can be made without interrupting the test. The fracture toughness is calculated by using the measured crack length and load with a compliance-crack length curve developed earlier.

Without the use of external lengthwise compression, both the longitudinal (T-L) and transverse (L-T) (ungrooved) aluminum specimens were directionally unstable while side-grooved samples were stable through the complete crack-growth range. The longitudinal specimens became unstable when the crack length $2a$ extended approximately 8.1 cm (3.2 in.). The distance to instability varied by only 5 percent between similar specimens. Referring to Fig. 5, the critical radius is determined to be $r_0 = r_c = 0.127$ mm (0.005 in.). Correspondingly, the instability in the ungrooved transverse test pieces occurred when $2a$ was approximately 6.86 cm (2.7 in.) and, thus, $r_0 = r_c = 0.25$ mm (0.010 in.). The dimensions observed for r_c appear to be slightly smaller than the plastic-zone size along $\theta = 0$ as determined by the numerical analysis of Larsson and Carlsson.[13] This result may be due to the fact that the predictions by Larsson and Carlsson are to the limit of the elastic-plastic interface. In reality, however, a finite amount of plastic deformation is required to initiate void nucleation from inclusions. Thus, we might expect that void or crack initiation will occur at distances somewhat smaller than the distance to the plastic interface. It could be argued that the critical radius to crack initiation in 7075-T651 aluminum, which predicts crack-path stability, is the maximum distance in which the ductile fracture process is active. Since this process involves plastic deformation, the maximum extent of the plastic zone along $\theta = 0$ should provide an approximate measure of r_c.

Now we consider the effect of stabilizing lengthwise stress on the measured toughness of the material. In Fig. 7, the fracture toughness K_c is plotted as a function A_2 minus the applied lengthwise stress. These results indicate that the critical stress intensity increases linearly with lengthwise tension. A least-squares program was used to determine the best linear fit to the experimental data. The 'degree of fit' or coefficient of determination η was also evaluated. When $\eta = \pm 1$, the correlation is said to be exact. When $\eta = 0$, the variables are said to be uncorrelated with a linear equation. A reasonably good linear fit is indicated in each case where $\eta = -0.767$, -0.872, and -0.682 for the T-L, L-T ungrooved, and L-T side-grooved specimens, respectively. Kibler and Roberts[5] similarly observed that the apparent fracture toughness increased with increasing biaxial loading on thin sheets. However, their results indicated that the biaxial dependence is much stronger than observed here. Furthermore, an increase in fracture toughness has been reported in several instances for cracks of increasing length in the DCB specimen.[14,15] As would be expected, the value of A_2/K_I increases with crack length in this specimen.

Using the result that the lengthwise stress influences the measured fracture toughness, it is worthwhile to point out certain implications. The ASTM compact tension and bend specimens have been developed to standardize K_{Ic} fracture testing. However, due to the difference in the two geometries, the A_2 stress term is not the same in both cases. Using a finite-element evaluation, Larsson and Carlsson[13] have shown that the ratio of $A_2/(K_I\sqrt{a})$ is 0.033 for the bend specimen and 0.291 for the compact tension specimen. In either case, the crack length is taken to be ½ the specimen width following the ASTM standard. Considering 7075-T651 aluminum with $S_y = 538$ MPa (78 ksi) and an apparent K_{Ic} of 27.5 MNm$^{3/2}$ (25.0 ksi-in.$^{1/2}$) for zero lengthwise stress (determined from the L-T side-grooved specimens, extrapolated to zero σ_x stress), we calculate that a reasonable specimen thickness and initial crack length is 10 mm (0.4 in.). Thus, K_I/A_2 can be determined from the Larsson and Carlsson work. Using the least-squares line for the relationship between K_c and σ_x developed from the center-cracked specimen, we can now calculate the expected value of K_c for each standard specimen:

$$K_c = (0.0239)(\sigma_x) + 27.5 \text{ MPa-m}^{1/2}$$

where the lengthwise stress σ_x is reported in MPa. For $\sigma_x = A_2$, that is, no externally applied stress, we find,

$$K_c = 27.5/[1 - 0.0239\ (A_2/K_I)] \text{ MPa-m}^{1/2}$$

where A_2/K_I is in m$^{-1/2}$.

Bend:

$$K_c = 27.6 \text{ MPa-m}^{1/2}, \quad A_2 = 3.6 \text{ MPa}$$

Compact Tension:

$$K_c = 28.3 \text{ MPa-m}^{1/2}, \quad A_2 = 32.6 \text{ MPa}$$

Using identical materials in the two different fracture tests, we expect to find a difference of approximately 2½ percent in the measured value of K_c, the CT specimen being slightly higher. Since scatter is inherently high in fracture testing, these differences would not be expected to be observed unless there were a large number of

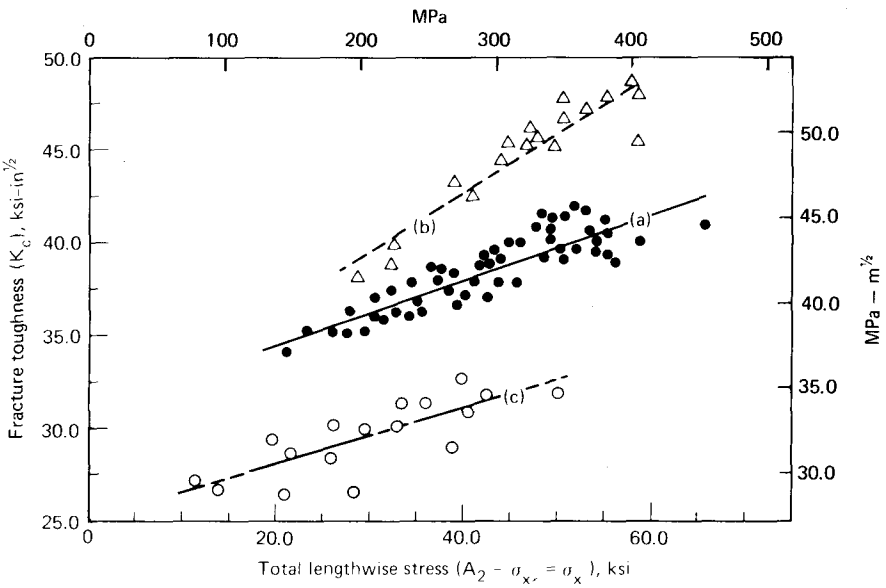

Fig. 7—7075-T651 fracture toughness as a function of the total lengthwise stress using the center-cracked specimen; (a) longitudinal orientation, no side grooves; (b) transverse orientation, no side grooves; and (c) transverse orientation with side grooves. Curve (c) closely approximates plane strain

identical samples made from the same material. Results from round-robin tests comparing the plane-strain fracture toughness of various high-strength materials using both the compact tension and bend specimens confirm that the differences in fracture toughness values are well within the experimental scatter.[16] However, it does appear that the overall results of the bend specimens are slightly lower than the compact specimens. In both cases, the bend and compact tension, the lengthwise term A_2 is much smaller than found in the DCB or center-cracked specimen.

Conclusions

The maximum circumferential-stress model which incorporates a critical distance to crack initiation can be used to describe the directional stability of crack growth in Mode I loading. The first two terms of the series expansion for the stresses near a Mode I crack, i.e., K_I and A_2 can be used to define a stability parameter r_0. We show that the value of the radius r_0 may be measured photoelastically by investigating the isochromatic-fringe geometry in the vicinity of a crack tip.

This directional-growth model is examined using a newly designed center-cracked specimen. Employing the criterion that directional instability occurs when the critical distance to crack initiation is greater than r_0, a correlation is drawn between the extent of the plastic zone along the crack plane and the crack-initiation distance r_c for ductile fracture of 7075-T651 aluminum. Further, using the center-cracked specimen, we find that the measured value of K_c is dependent upon the stress parallel to the crack plane, i.e., A_2. The value of this stress term can be altered by an external lengthwise stress. Application of sufficient lengthwise compression increases r_0 and therefore establishes specimen stability in an otherwise directionally unstable configuration.

Acknowledgment

The authors greatly appreciate the support of the University of California, Lawrence Livermore Laboratory. Special thanks are directed to Jack Stone for help in carrying out the photoelastic work.

"Work performed under the auspices of the U.S. Department of Energy by the Lawrence Livermore Laboratory under contract number W-7405-ENG-48."

References

1. Berry, J.P., "Determination of Fracture Surface Energies by the Cleavage Technique," J. Appl. Phys., 34, 62-68 (Jan. 1963).

2. Kirkwood, W.F. and Prado, M.E., "Three Dimensional Stress Distribution of a Double-Cantilever Beam with a Side Notch," Cracks and Fracture, ASTM 601, 262-273 (1976).

3. Benbow, J.J. and Roesler, F.C., "Experiments on Controlled Fractures," Proc. Phys. Soc. (London), 70, Ser. B., 201-211 (1957).

4. Saith, A., "On The Stability and Arrest of Cracks," Ph.D. Thesis, University of California, Berkeley, CA (1971).

5. Kibler, J.J. and Roberts, R., "The Effect of Biaxial Stresses on Fatigue and Fracture," ASME Trans. J. of Engin. Ind., 727-734 (1970).

6. Erdogan, F. and Sih, G.C., "On the Crack Extension in Plates Under Plane Loading and Transverse Shear," J. Basic Eng., Trans. ASME, 85, Ser. D., 519-527 (Dec. 1963).

7. Williams, J.G. and Ewing, P.D., "Fracture Under Complex Stress - The Angled Crack Problem," Int. J. Fract. Mech., 8 (4), 441-446 (Dec. 1972).

8. Finnie, I. and Saith, A., "A Note on the Angled Crack Problem and the Directional Stability of Cracks," Int. J. of Fract., 9, 484-486 (1973).

9. Rice, J.R. and Johnson, M.A., "The Role of Large Crack Tip Geometry Change in Plane Strain Fracture," In Elastic Behavior of Solids, McGraw-Hill, 641-672 (1970).

10. Richie, R.O., Knott, J.F. and Rice, J.R., "On the Relationship Between Critical Tensile Stress and Fracture Toughness in Mild Steel," J. Mech. Phys. Solids, 21, 395-410 (1973).

11, Irwin, G.R., "Analysis of Stresses and Strains Near the End of a Crack Traversing a Plate," J. Appl. Mech., 24 (3), 361-364 (1957).

12. Creager, M. and Paris, P., "Elastic Field Equations for Blunt Crack with Reference to Stress Corrosion Cracking," Int. J. Fract., 3 (4), 247-251 (1967).

13. Larsson, S.G. and Carlsson, A.J., "Influence of Non-Singular Stress Terms and Specimen Geometry on Small Scale Yielding at the Crack Tip in Elastic-Plastic Materials," J. Mech. Phys. Solids, 21, 263-277 (1973).

14. Perra, M.W. and Finnie, I., "Fracture Toughness of a High Strength Beryllium at Room Temperature and 300 C Degrees," J. of Matls. Science, 12, 1519-1526 (1977).

15. Nelson, F.G., Schilling, P.E. and Kaufman, J.G., "The Effect of Specimen Size on the Results of Plane-Strain Fracture-Toughness Tests," Engin. Fract. Mech., 4, 33-50 (1972).

16. McCabe, D.E., "Evaluation of the Compact Tension Specimen for Determining Plane Strain Fracture Toughness of High Strength Materials," J. of Matls., 7 (4), 449-454 (Dec. 1972).